

Development of tool life prediction system for square end-mills based on database of servo motor current value

Hiroyuki KODAMA*, Makoto SUZUKI** and Kazuhito OHASHI*

* Faculty of Environmental, Life, Natural Science and Technology, Okayama University

3-1-1, Tsushima-naka, Kita-ku, Okayama-shi, Okayama, 700-8530, Japan

E-mail: h-kodama@okayama-u.ac.jp

** Graduate school of Environmental, Life, Natural Science and Technology, Okayama University

3-1-1, Tsushima-naka, Kita-ku, Okayama-shi, Okayama, 700-8530, Japan

Received: 19 September 2024; Revised: 14 November 2024; Accepted: 11 December 2024

Abstract

Accurate prediction of tool life is crucial for reducing production costs and enhancing quality in the machining process. However, such predictions often rely on empirical knowledge, which may limit inexperienced engineers to reliably obtain accurate predictions. This study explores a method to predict the tool life of a cutting machine using servo motor current data collected during the initial stages of tool wear, which is a cost-effective approach. The LightGBM model was identified as suitable for predicting tool life from current data, given the challenges associated with predicting from the average variation of current values. By identifying and utilizing the top 50 features from the current data for prediction, the accuracy of tool life prediction in the early wear stage improved. As this prediction method was developed based on current data obtained during the very early wear stage in experiments with square end-mills, it was tested on extrapolated data using different end-mill diameters. The findings revealed average accuracy rates of 71.2% and 69.4% when using maximum machining time and maximum removal volume as thresholds, respectively.

Keywords : Milling, LightGBM, Tool life prediction, Square end-mill, Servo motor current

1. Introduction

The increasing demand for reduced manufacturing costs, enhanced processing accuracy, and diminished environmental impacts has signified the importance of estimating tool wear and developing predictive methods for tool life in the cutting industry (Nouri et al., 2015; Azeem, 2007). Numerous studies have addressed this issue. For instance, a common approach involves performing a frequency analysis of cutting resistance and tool vibration acceleration data, collected via a dynamometer, to identify the key factors influencing tool wear progression to isolate the frequency components correlating with the extent of wear (Dimla and Lister, 2000; Mecheri et al., 2010).

Additionally, several researchers have explored the application of machine learning techniques to cutting resistance values or vibration data gathered during processing to accurately estimate and predict tool wear (Krishnakumar et al., 2018; Jie et al., 2014). For example, Xu et al. (2014) developed a tool wear prediction system using a back-propagation neural network (BPNN) based on cutting resistance data obtained during drilling. Similarly, Liu et al. (2020) developed a system for assessing tool degradation by applying a deep learning method known as long short-term memory (LSTM), which is adept at handling time series data, to vibration acceleration waveform data characterized by substantial non-stationary and non-linear noise.

Despite their high accuracy in tool life assessments, dynamometers present challenges such as chatter vibration, dimensional errors caused by the reduced machine tool rigidity, lack of overload protection, and high implementation costs (Li et al., 2005). Consequently, research has explored alternative methods such as using current values from servo motors, which are relatively inexpensive and do not require additional sensors. For instance, Li et al. (2000) estimated cutting resistance from servo motor current to monitor tool wear, and Salimi et al. (2012) predicted tool life by estimating current values from spindle and table feed servo motors. Nevertheless, prior studies have reported that current data are

significantly affected by noise from friction and viscous damping in the machine tool table, and filtering can result in the loss of high-frequency component features, rendering them unsuitable for estimating tool wear conditions (Rizal et al., 2014). Consequently, various methods have been proposed employing machine learning techniques on current data to more effectively estimate tool wear.

For instance, Ghosh et al. (2007) fused features extracted from signal data, such as cutting resistance, spindle vibration, and spindle current value, and applied them to a convolutional neural network (CNN) to develop a system for estimating the average flank wear on the cutting edge of a tool. Additionally, Nie et al. (2022) devised a method that utilized CNN and bidirectional LSTM (BiLSTM) to analyze current value data during processing to extract features indicative of tool wear. Recent research including that by Wang et al. (2021) has increasingly focused on predicting tool life using ensemble learning methods, which are machine learning techniques based on decision tree algorithms. Among these, the light gradient boosting machine (LightGBM) model has been validated as more accurate in prediction than other decision tree-based models such as the extreme gradient boosting (XGBoost) model and the random forest (RF) model (Mahmood, 2022). Li et al. (2020) reported that a system trained on LightGBM using vibration, current value, and cutting resistance data proved effective in predicting tool wear.

Despite the variety of approaches to tool life prediction and estimation of tool wear based on current data, several issues persist: (1) Current value data from the entire processing period—from the onset to the end of the tool's life—are required for accurate tool life prediction. (2) Even if the stage at which tool life is reached is accurately predicted, the tool tip shape may no longer be maintained, likely affecting the characteristics of the cutting surface adversely. (3) Ideally, tool life prediction should use servo motor current value data from conditions where the tool tip has minimal wear ("very early wear stage"), but there is no established method to maintain prediction accuracy and generalization performance under these conditions. (4) No previous studies have visualized and quantified the correlation between the features in the database and their relationship with tool life prediction. In particular, specific examples have not been presented in the literature that address research focused on predicting the future cutting time and material removal volume leading up to tool end-of-life by using current data obtained during machining when the tool edge exhibits minimal wear (essentially in a near-new condition).

Therefore, this study aims to address these issues by inputting current value data from very early wear conditions to develop a system that predicts tool wear conditions with high accuracy at arbitrarily set cutting times and material removal volumes. We conduct cutting experiments using a square end-mill that is commonly employed in a broad range of applications and simulates the rough machining of mass-produced products. We employ the LightGBM model on experimentally obtained current value data. The effectiveness of the system is verified by evaluating the prediction accuracy using processing data (extrapolated data) for different tool diameters not included in the training set. Additionally, we quantify and discuss significant features inherent in the current value data for tool life prediction.

		Predicted Class	
		Negative	Positive
Actual Class	Negative	<i>TN</i> (True Negative)	<i>FP</i> (False Positive)
	Positive	<i>FN</i> (False Negative)	<i>TP</i> (True Positive)

$$\left\{ \begin{aligned} \text{ACR} &= \frac{TP + TN}{TP + FP + TN + FN} \\ \text{TPR} &= \frac{TP}{TP + FN} \\ \text{TNR} &= \frac{TN}{FP + TN} \end{aligned} \right.$$

Fig. 1 A mixed matrix is used to calculate the correct response rate, true positive rate, and true negative rate. The correct response rate represents the percentage of accurately predicted data overall, while the true positive rate indicates the percentage of correctly predicted positive data, and the true negative rate shows the percentage of correctly predicted negative data.

2. Machine learning algorithm for tool life prediction

2.1 Evaluation indicators for prediction accuracy

In this study, we employed the accuracy rate, true positive rate, and true negative rate as evaluation metrics. Figure 1 illustrates the confusion matrix utilized to calculate these metrics. In binary classification via machine learning, labels are categorized as either positive or negative. A true positive (TP) occurs when positive instances are correctly identified as positive. A false positive (FP) occurs when negative instances are incorrectly identified as positive. A true negative (TN) occurs when negative instances are correctly identified as negative. A false negative (FN) occurs when positive instances are incorrectly identified as negative.

The confusion matrix, as depicted, categorizes these outcomes based on the actual and predicted labels. These values facilitate the computation of the accuracy rate (ACR), true positive rate (TPR), and true negative rate (TNR). Specifically, ACR represents the proportion of correct predictions across all data, TPR and TNR represent the proportion of positive and negative instances correctly identified as positive and negative, respectively.

2.2 LightGBM model

LightGBM is an ensemble learning method based on decision trees. High-precision decision tree-based ensemble learning methods, such as XGBoost and Random Forest (RF), have been established for some time. LightGBM incorporates techniques from these existing methods, as well as gradient-based one-side sampling and exclusive feature bundling, to enhance the new gradient boosting decision tree method (Ke et al., 2017). This method is prevalently used in machine learning competitions, including those on Kaggle.

Decision tree methods such as LightGBM can quantitatively assess the contribution of features to a prediction through a metric known as "importance." The calculation of importance is demonstrated using the K-class classification decision tree depicted in Fig. 2. The calculation begins with determining the Gini impurity. The Gini impurity $G(a)$ at a specific node a is defined as Eq. (1):

$$G(a) = \sum_{i=1}^k p(i)(1 - p(i)) \quad (1)$$

$$p(i) = \frac{N_i}{N_a} \quad (2)$$

where $p(i)$ represents the frequency of class i in node a , and N_a and N_i represent the number of data in node a and class i , respectively. The aforementioned equation expresses that the Gini impurity $G(a)$ is smaller when the data in node a are biased toward a single label. Thus, the Gini impurity can be used to quantitatively evaluate the purity of a label in each node. Focusing on the parent node P and child nodes R and L constituting the K-class decision tree, the importance $I(v)$ of a given feature v can be defined using Eq. (3) as follows:

$$I(v) = \sum_{j=1}^{m \in F(v)} \{N_P(j)G_P(j) - N_R(j)G_R(j) - N_L(j)G_L(j)\} \quad (3)$$

where $F(v)$ represent the set of nodes divided by feature v . This equation indicates that the importance of a feature is a quantitative representation of how much the Gini impurity can be reduced when dividing from a parent node to a child node. The decision tree feature known as the "class classification method" is deemed appropriate for analytical purposes, and its capability to visualize feature importance is considered beneficial for enhancing accuracy through the interpretation of analytical results and examination of their relationship with processing phenomena. Implementing the LightGBM model demands the configuration of various analysis parameters, or hyperparameters, which are summarized in Table 1. For this analysis, the "binary" option was selected to classify whether the tool life under each cutting condition exceeds a predetermined threshold.

Table 1 Hyperparameters

Calculations when using boosting methods	gbdt
Parameters for specifying a task	binary
Learning rate	0.1
Maximum number of leaves on the decision tree	50
Number of data that can go into one leaf	10
Maximum number of calculations	1000

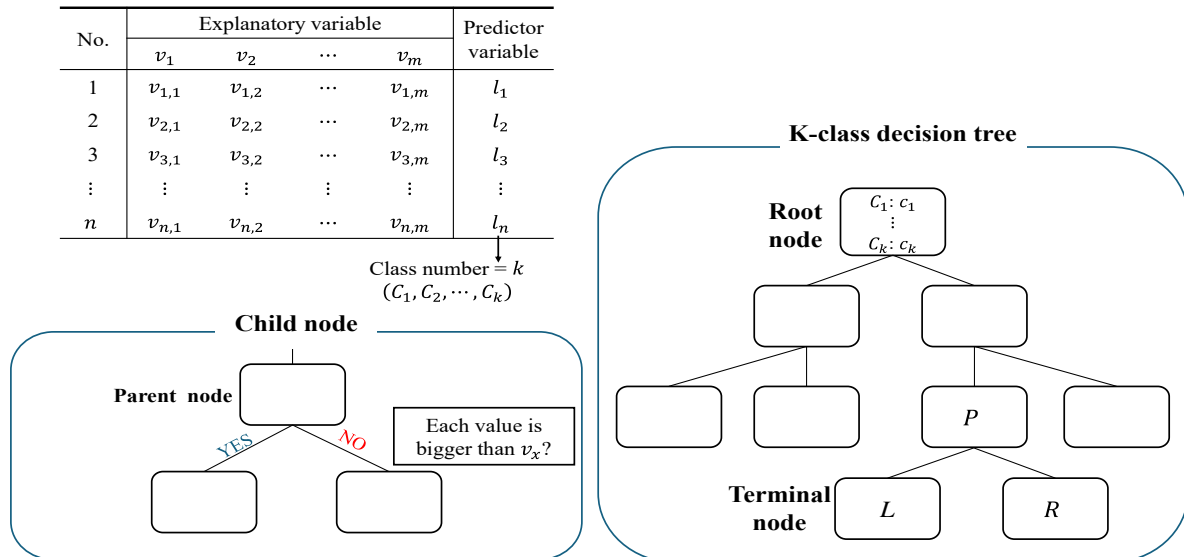


Fig. 2 The decision tree method transforms tabular data with one-to-one correspondence between explanatory variables (feature groups) and target variables into a tree structure.

3. Prediction of tool wear conditions using current value data under very early wear stage conditions

3.1 Overview of definition of very early wear stage conditions and tool wear prediction method

In this study, "very early wear stage" are defined as scenarios where the flank wear width V_B of the tool tip post-processing is 0.01 mm or less. Therefore, when visually inspecting the wear width of the tool tip in the "very early wear stage," it is nearly indistinguishable from the wear-free, new condition of the tool tip. Figure 3 illustrates a model diagram that delineates these conditions based on shifts in cutting distance and flank wear width V_B . As assumed, the tool reaches its end of life at L_{life} [mm]. Section 3.2 details cutting experiments that indicate $L_{life}/500$ [mm] (cutting distance: ~100 mm) as an average benchmark for the cutting distance section representing very early wear stage conditions. Figure 4 provides an overview of the method used to predict tool wear conditions from servo motor current value data during the very early wear stage. This method is segmented into three major parts: (a) preprocessing, (b) prediction, and (c) improvement.

In the preprocessing part, tool wear under each cutting condition is labeled as either above or below a set threshold. If the tool wear indicates that the tool life has not been reached, it is labeled "OK" for continued use; otherwise, it is labeled "NG" for discontinuation. These labels will be consistently used throughout the study. Users set an arbitrary threshold for cutting time t [min] or removal volume V [mm³], and label whether the tool life exceeds this threshold during experiments under each cutting condition. Subsequently, the current value data, converted into feature data using the tsfresh library—a prominent feature extraction method provided by Python3—are linked with the aforementioned labels to create the training database. The tsfresh library facilitates the transformation of time series data into various statistical features, such as variance, standard deviation, skewness, and Fourier coefficients. This database is then employed to train the LightGBM model.

A test database was constructed by converting the current value data obtained under the very early wear stage

conditions for each cutting scenario into feature data and establishing a correspondence with the previously mentioned labels. In this analysis, the current value feature data serves as the explanatory variable, whereas the objective variable is whether the tool life exceeds a specified threshold. This method employs a current value feature database, which is compiled from data gathered under various cutting conditions and tool diameters, to train the LightGBM model. The model predicts the tool wear state from data collected in the very early wear stage, where the tool exhibits minimal wear. The method assesses whether the predicted outcomes surpass a user-defined threshold, thus enabling the estimation of the end-mill's cutting time and material removal volume based on the current value data from the initial wear stage. The prediction results are evaluated using the metrics of ACR, TPR, and TNR. Additionally, the relationship between features is examined through the visualization of feature importance, and the findings are discussed in relation to the cutting mechanism and other factors. The results and discussions inform considerations for improving accuracy, which are subsequently integrated into the preprocessing phase for a second analysis.

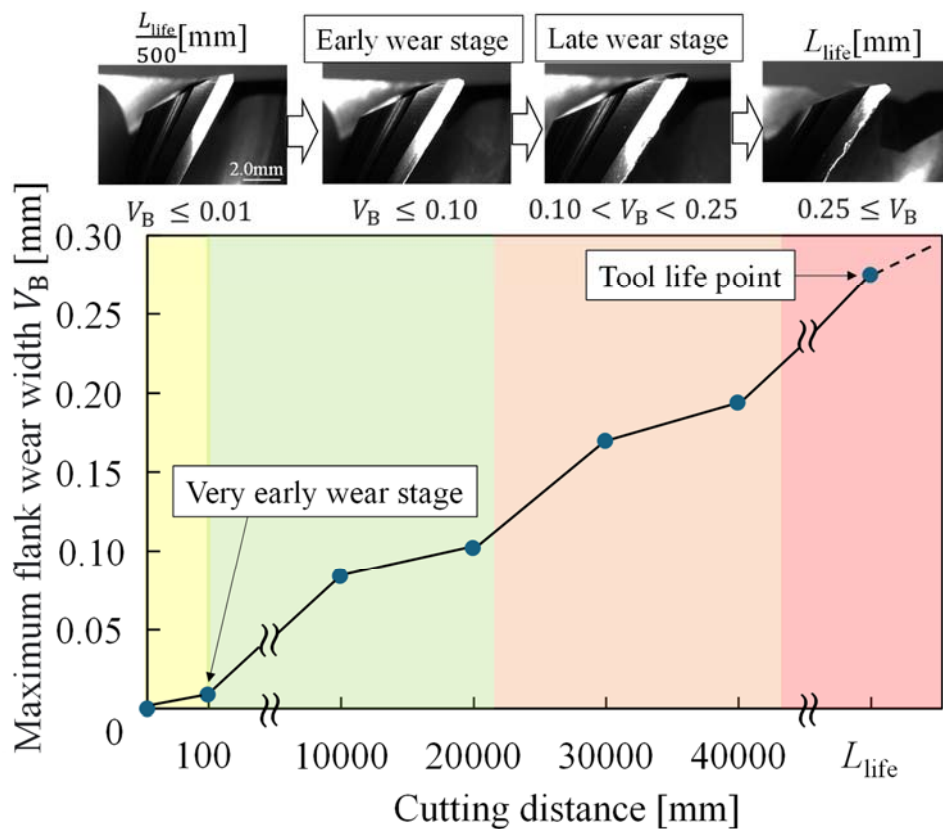


Fig. 3 Model diagram defining the very early wear stage conditions based on the cutting distance and the flank wear width V_B .

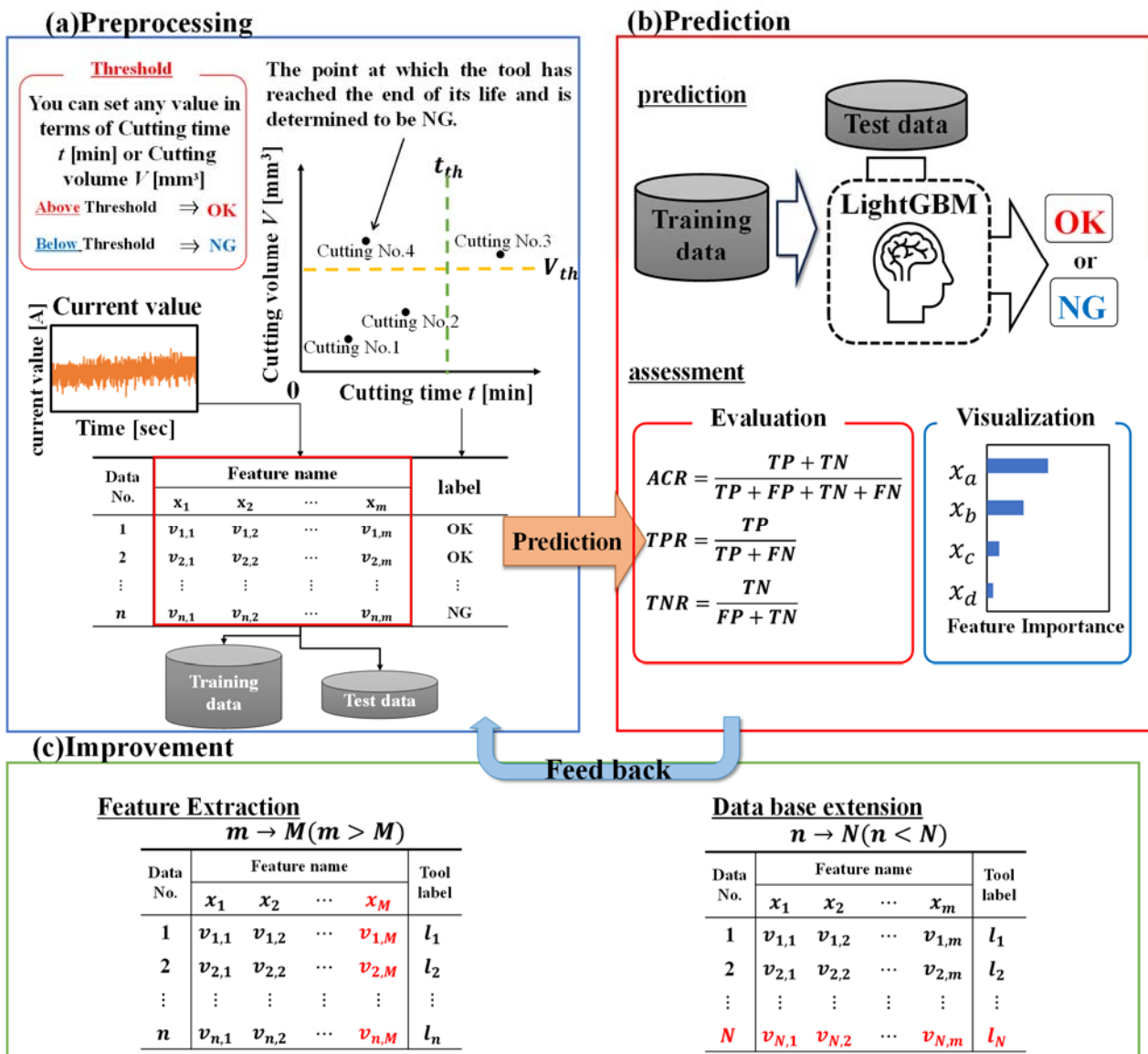


Fig. 4 At the very early stage of machining, tool life prediction from servo motor current data involves three main steps: (a) Pre-processing, (b) Prediction, and (c) Improvement.

Table 2 Experimental conditions

Machine tool	YAMASAKI GIKEN: YZ-402-HR
NC device	FANUC: 31i-MODEL B
Work material	JIS S45C (HRC:27)
Tool	NEW CENTURY: 4NV-30D-8.0
	NEW CENTU-RY: 4NV-30D-10
	NEW CENTU-RY: 4NV-30D-12
	Number of flutes: 4 Coating: AlCr Helix angel: 35[°], 37[°]
Holder	SCHUNK: BT40-20
Coolant	TAIYU: TPP-ZERO + highly alkaline water

Table 3 Cutting conditions
(a) $\phi 8$ Square end-mill

Condition No.	Spindle speed S [rpm]	Table feed F [mm/min]	Radial depth of cut ae [mm]	Axial depth of cut ap [mm]
1	3193	294	1.4	12
2	3193	294	2.4	20
3	3193	294	3.4	24
4	3193	490	1.4	20
5	3193	490	2.4	24
6	3193	490	3.4	12
7	3193	686	1.4	24
8	3193	686	2.4	12
9	3193	686	3.4	20
10	5322	294	1.4	12
11	5322	294	2.4	20
12	5322	294	3.4	24
13	5322	490	1.4	20
14	5322	490	2.4	24
15	5322	490	3.4	12
16	5322	686	1.4	24
17	5322	686	2.4	12
18	5322	686	3.4	20
19	7450	294	1.4	12
20	7450	294	2.4	20
21	7450	294	3.4	24
22	7450	490	1.4	20
23	7450	490	2.4	24
24	7450	490	3.4	12
25	7450	686	1.4	24
26	7450	686	2.4	12
27	7450	686	3.4	20

(b) $\phi 10$ Square end-mill

Condition No.	Spindle speed S [rpm]	Table feed F [mm/min]	Radial depth of cut ae [mm]	Axial depth of cut ap [mm]
1	3765	488	2.4	20
2	4706	610	3.0	25
3	5647	732	3.6	30
4	3765	610	3.6	18
5	4706	488	2.4	18
6	5647	732	3.0	18

(c) $\phi 12$ Square end-mill

Condition No.	Spindle speed S [rpm]	Table feed F [mm/min]	Radial depth of cut ae [mm]	Axial depth of cut ap [mm]
1	2353	377	2.2	18
2	2353	377	3.6	30
3	2353	377	5.0	36
4	2353	629	2.2	30
5	2353	629	3.6	36
6	2353	629	5.0	18
7	2353	881	2.2	36
8	2353	881	3.6	18
9	2353	881	5.0	30
10	3921	377	2.2	18
11	3921	377	3.6	30
12	3921	377	5.0	36
13	3921	629	2.2	30
14	3921	629	3.6	36
15	3921	629	5.0	18
16	3921	881	2.2	36
17	3921	881	3.6	18
18	3921	881	5.0	30
19	5489	377	2.2	18
20	5489	377	3.6	30
21	5489	377	5.0	36
22	5489	629	2.2	30
23	5489	629	3.6	36
24	5489	629	5.0	18
25	5489	881	2.2	36
26	5489	881	3.6	18
27	5489	881	5.0	30

3.2 Experimental method for database acquisition

Figure 5 provides an overview of the cutting experiment. The work materials for wear and measurement were secured on the machine tool table using a jig. Initially, the servo motor current values and resistance values for each table axis were measured when cutting the measurement material in the Y-axis direction for one pass, followed by capturing an image of the tool wear. Subsequently, the wear material was cut using a square end-mill over a distance of 10,000 mm. After this cutting phase, the measurement material was again cut for one pass (cutting distance: 100 mm), and various data were collected before another tool wear image was captured. Tool conditions were assessed based on the wear width $V_B = 0.25$ mm parallel to the flank.

When $V_B < 0.25$ [mm], the tool was deemed acceptable for continued use, and labeled with “OK”. When $V_B \geq 0.25$ [mm], the tool was deemed unacceptable for continued use, and labeled with “NG”. This process was repeated for each 10,000 mm segment cut. The experimental conditions are listed in Table 2. The machine tool used was a triaxial orthogonal machining center (Yamasaki Giken YZ402HR), and the NC device was the 31i-MODEL B (FANUC). The work material was JIS S45C (HRC: 27).

We utilized three different tool diameters ($\phi 8$, $\phi 10$, $\phi 12$) with a BT40 holder for a square end-mill (NEW CENTURY) in our experiments. These tools are well-established in the industry. The experiments were conducted using both down cutting and side-milling method as depicted in Fig. 6. The cutting parameters included spindle speed (S), table feed (F), radial depth of cut (ae), and axial depth of cut (ap), as detailed in Table 3. The cutting conditions for the $\phi 8$ and $\phi 12$ square end-mills were established based on the standard conditions provided in the tool catalogs, which were (S



Fig. 5 Experimental setup displaying a jig that fixes the workpiece for wear and the workpiece for measurement on the machine tool table.

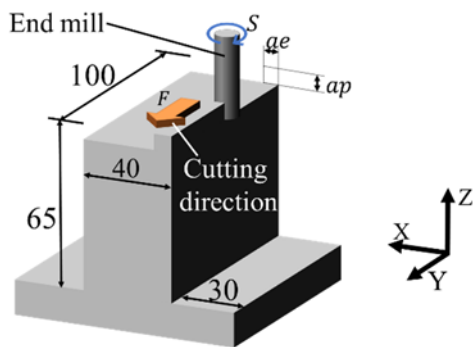


Fig. 6 Cutting was accomplished through down-cutting with side milling.

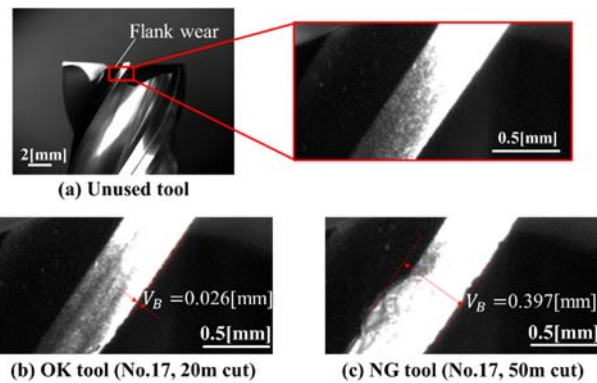


Fig. 7 Figures below demonstrate an example of a tool that has been evaluated as either acceptable (OK) or not acceptable (NG).

= 5322 rpm, $F = 490$ mm/min, $ae = 2.4$ mm, $ap = 20$ mm). These conditions were adjusted to three levels (original values and $\pm 40\%$) according to an L27 orthogonal array with four factors at three levels. For the standard conditions, +40% was set assuming high-efficiency rough machining, and -40% as finishing machining.

For the $\phi 8$ square end-mill, the third level of axial depth of cut (ap) would be $20 \times 1.4 = 28$ mm. However, owing to the tool overhang limitations, this value was adjusted to 24 mm. Figure 7 illustrates examples of tools categorized as acceptable (OK) or not acceptable (NG) in experiment 17 using a $\phi 8$ square end-mill, showing images at cutting distances of 20,000 mm (20 m) and 50,000 mm (50 m).

Figure 8 presents the relationship between cutting distance, tool wear, cutting resistance, and the average amplitude of the table axis servo motor current until the tool life endpoint, using data from experiment 27 with a $\phi 12$ square end-mill. The cutting resistance was calculated by taking a moving average of the values at each distance, with the maximum value serving as the representative evaluation metric. The sampling period was 0.0002 s, and the average number of moving average values was 10. Figure 8 reveals that tool flank wear consistently progresses with the increase in the cutting distance. With tool flank wear, the primary component of cutting resistance, particularly the principal force, F_x , increases, and a slight upward trend can be observed in the average amplitude of the current. This phenomenon indicates that the fluctuations in the average amplitude of the Y-axis servo motor current exhibit a trend similar to that of the fluctuating components of the principal force observed during machining. These trends were consistent across all tested cutting conditions.

In all conditions, the flank wear width V_B (average of four blades) at the tool tip after processing the work material for one pass (cutting distance: 100 mm) was below 0.01 mm, indicating very early wear stage conditions. Notably, the $\phi 8$ square end-mill (experiment number 11) demonstrated a relatively longer cutting distance in terms of the flank wear

width until the tool life was reached compared to other conditions. For this specific case, considering potential biases in the training database, the usability limit of the tool was determined when the principal force component (F_x) of the cutting resistance approximately doubled from the very early stage where minimal flank wear was observed (Kakino et al., 2000). The instances where the tool chipped or broke prematurely were classified as “NG” at that stage.

Figure 9 presents an overview of the control method for the machine tool table and the method for acquiring servo motor current data. The machine tool, depicted in Fig. 7, was driven by ball screws in three directions (x, y, z) and controlled by the torque from a servo motor. This servo motor was governed by CNC commands. The current values of the servo motor for each axis (x, y, z) during operation were recorded by connecting the CNC to a PC equipped with FUNUC: SERVO VIEWER software via Ethernet.

Figure 10 illustrates the method for acquiring images of the tool. After processing, the tool was removed from the spindle and placed on a tool pre-setter (Kyoritsu Seiki: HP-6040V). The images were captured using a preset imaging program, focusing on the boundary wear area, tool tip (flank, rake), and tool top surface, as indicated in Fig. 10. The distance from the camera to the imaged areas was consistently 258 mm. This tool pre-setter facilitated visual inspection of wear in the micrometer range.

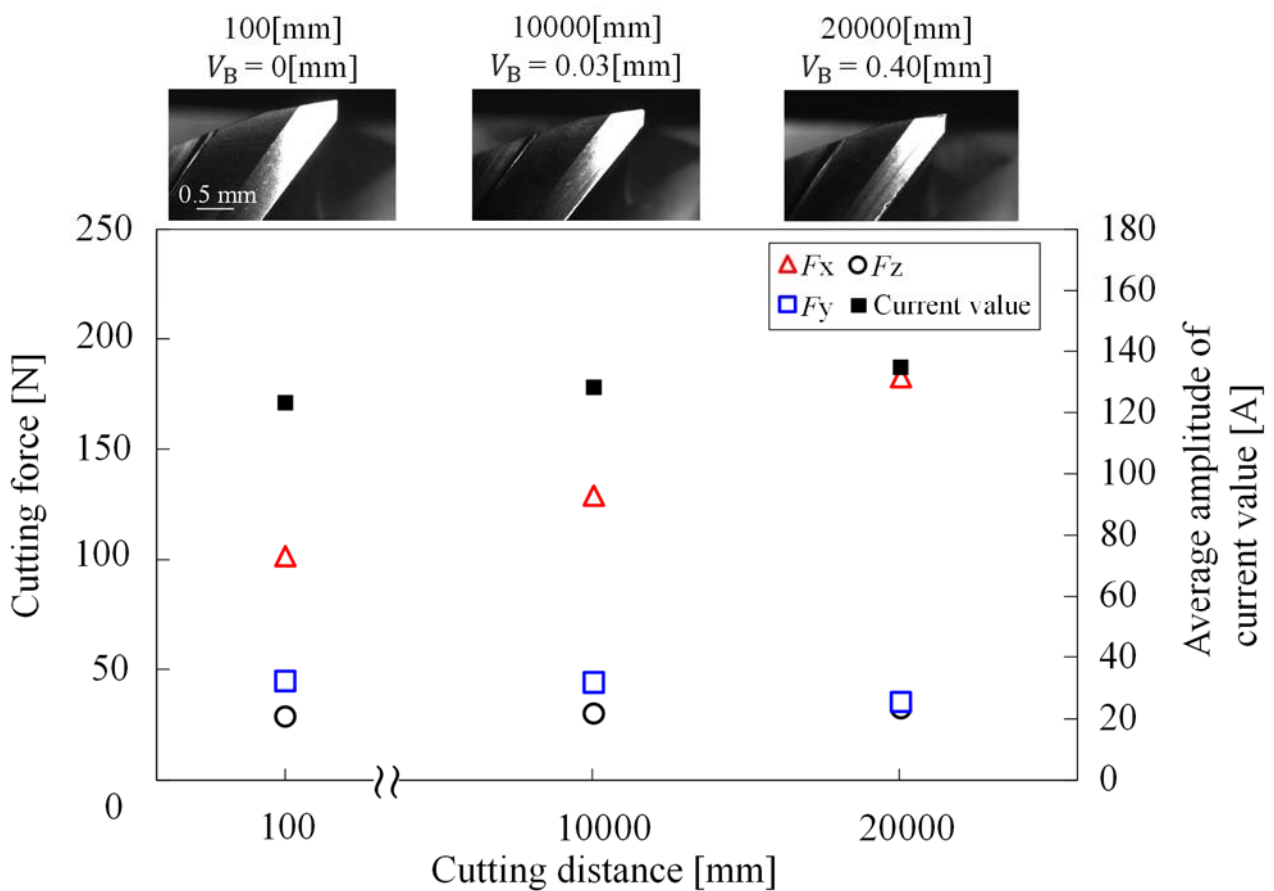


Fig. 8 Measured cutting force, average amplitude of current value and tool wear evolution for the $\phi 12$ square end-mill condition (experiment No. 27), which was the subject of the test data.

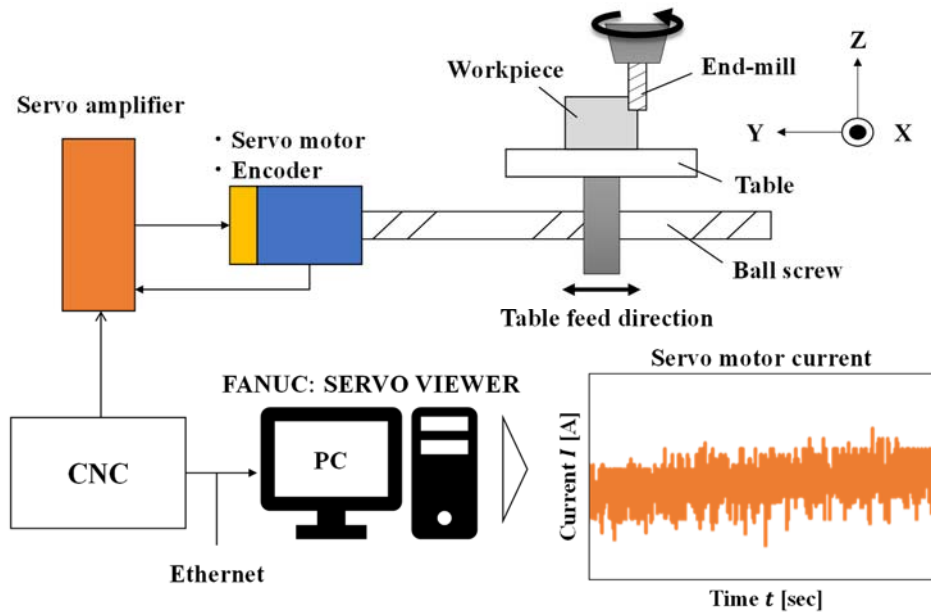


Fig. 9 Schematic of the control method of a machine tool table and the method of acquiring servo motor current data. Machine tool used in this study is driven by a ball screw and controlled by applying torque with a servo motor.

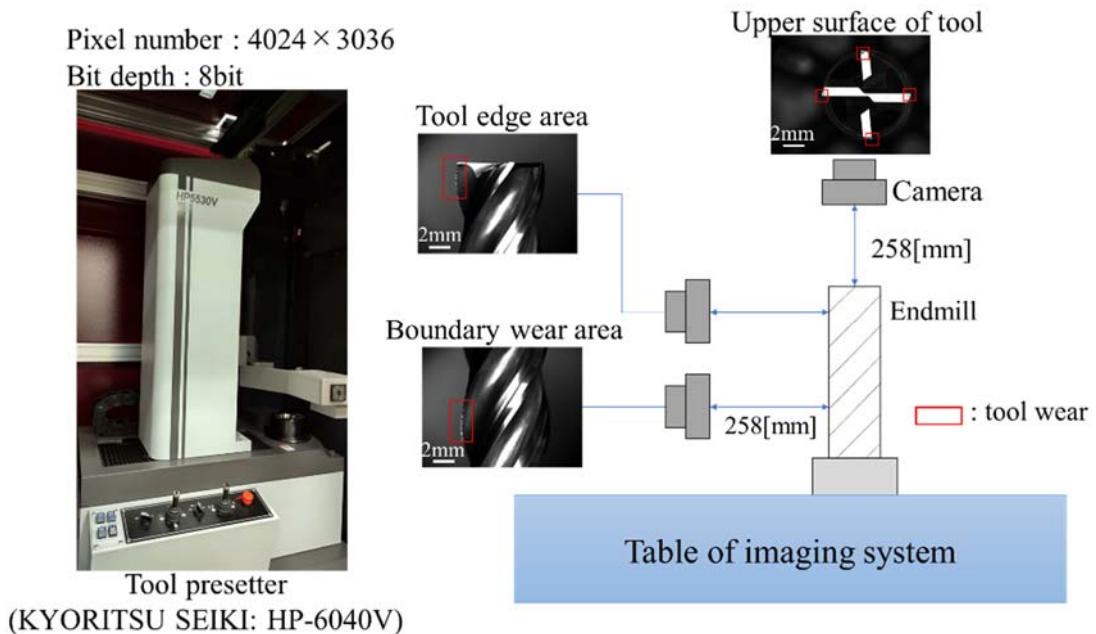


Fig. 10 Figure below is a schematic of the tool photograph acquisition method. Right: images of boundary wear area, tool tip (flank and rake surfaces, boundary wear area), and Upper surface of the tool.

3.3 Labeling of cutting conditions and threshold selection criteria

Figure 11 illustrates the tool life judgment diagram, hereinafter referred to as tool life points. As illustrated, users can set arbitrary thresholds for cutting time (t_{th}) and removal time (V_{th}) to determine if the tool life under each cutting condition exceeds these thresholds. In this study, the threshold t_{th} was established at four levels based on the mean, median, first quartile, and third quartile for the maximum cutting time (t). The threshold V_{th} was determined by calculating the removal volume at threshold t for each cutting condition, averaging these volumes, and setting four thresholds based on these averages.

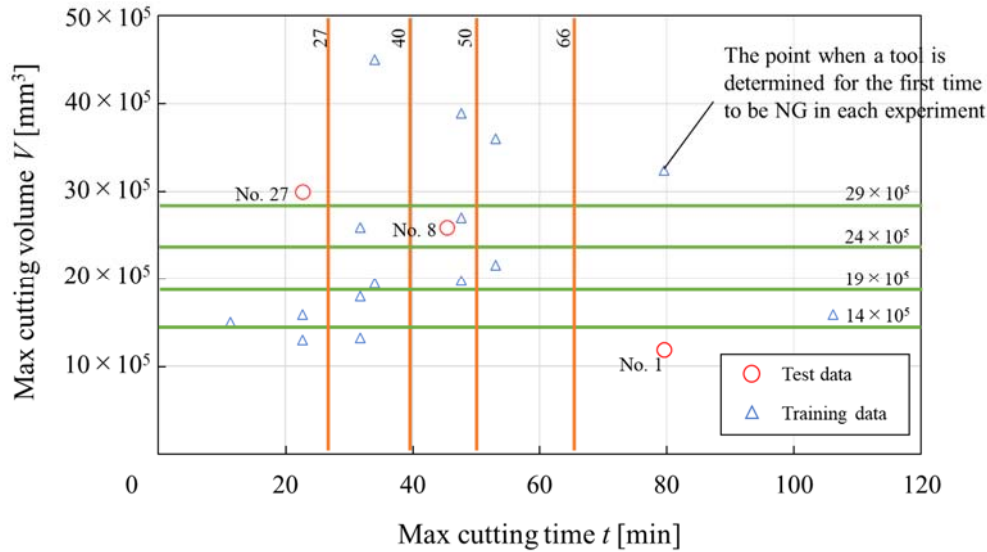


Fig. 11 Tool life judgment chart is a graph displaying the relationship between the tool life time, maximum machining time t and maximum removal volume V . Chart helps to determine if the tool life for a particular cutting condition exceeds a threshold value set by the user for the machining time and removal volume.

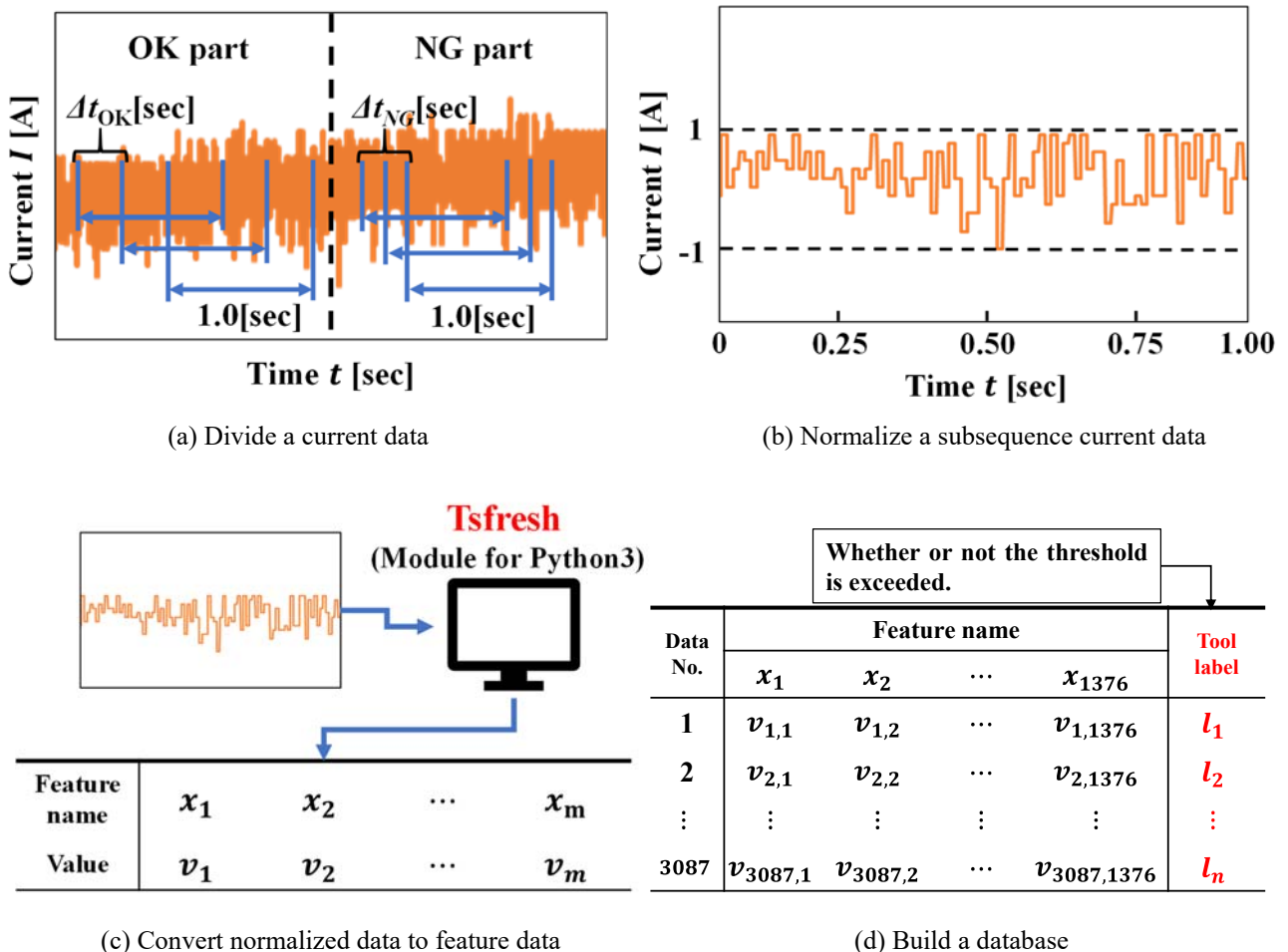


Fig. 12 Data obtained during processing is divided into intervals of 1.0s, and each interval is normalized to have a maximum value of 1 and a minimum value of -1 . Resulting data is processed using a package called tsfresh to extract features. This process creates a database consisting of n data points and m features. Database is associated with a tool life judgment (OK/NG) for each data acquisition.

3.4 Data preprocessing and database construction for application of machine learning methods

The preprocessing and database construction method for converting time-series current value data into feature data suitable for LightGBM is described here. Although the load meter value (current amplitude value) can be obtained from SERVO VIEWER, excessive load readings were observed during non-processing activities such as spindle rotation and stopping because of high detection sensitivity. Consequently, the data from these periods must be excluded, which prolongs the analysis time. Moreover, the spindle load meter value fluctuates significantly with variations in spindle speed, processing load, and tool diameter. These fluctuations, more pronounced than the progression of tool wear, complicate the construction of a versatile database. Therefore, the servo motor current values from the table motion axes, which exhibit lower detection sensitivity, were selected for the tool life prediction database. The data acquisition was performed for the x , y , and z table axes. However, the analysis verified that the y -axis servo motor current value was most significant for predicting tool life, leading to the exclusive use of y -axis current value data in the database.

First, to conduct various analyses from the current value data during processing, the current value data during non-processing were eliminated, and only the current value data during the processing were extracted. Figure 12 displays the method for converting the current value data from time series data to feature data. The current value data during processing were divided into 1.0 s sections, as depicted in Fig. 12(a). Additionally, the division widths were shifted every Δt [s], which enabled the extraction of multiple current value datasets with a length of 1.0 [sec]. The maximum cutting edge passing frequency in this experiment was 497 [Hz], so dividing the data every 1.0 [sec] can sufficiently include fluctuations in the current value data that occur when the tool interferes with the work material. Additionally, the division width shift amount Δt [s] depends on whether the tool life judgment for the current value data is OK or NG. In case of OK, the value is $\Delta t_{OK}=0.25$ [s], and based on the number of OK and NG labels N_{OK} and N_{NG} , respectively, for that cutting condition, the value in case of NG is calculated as $\Delta t_{NG} = \Delta t_{OK}(N_{NG}/N_{OK})$. This method reduces the division width shift amount in the NG data, which results in the overall ratio of OK and NG division current value data being roughly equal. During predictions, biases between data labels can reduce prediction accuracy and hinder interpretation of feature importance, so this type of processing was conducted. Afterwards, as portrayed in Fig. 12(b), each division current value dataset was normalized such that the minimum and maximum values were -1 and 1 , respectively. The normalization process enables us to reduce noise that results in irregular fluctuations in the bandwidth of the servo motor current value owing to factors such as the machine tool operation time and atmosphere of the work site. As portrayed in Fig. 12(c), each normalized division current value dataset was converted to feature data by applying tsfresh, which is available in Python3. These steps (a)–(c) to all the current value data obtained in the experiment are applied to create a database with a number of datasets n and number of features m , as depicted in Fig. 12(d). Additionally, as displayed in the same figure, the tool wear state judgment OK or NG when each dataset is obtained is labeled in the database.

3.5 Current value feature extraction method that considers importance with regards to prediction

The application of tsfresh enables the extraction of 1,376 features from each current value data point during processing (3,087 items), which were obtained under various cutting conditions for all tool diameters. Assuming that features are selected without duplication at each branch in the LightGBM model's decision tree, and considering that the tree has 50 leaves, the approximate number of possible feature combinations is $2^{50} \times {}_{1376}C_{50} \cong 1.28 \times 10^{107}$. However, in practice, this number is lower because features that do not contribute to prediction are also included. Given this vast number of combinations, the original dataset is relatively small, potentially deteriorating the prediction accuracy and generalization performance. Therefore, the number of feature combination patterns need to be reduced by effectively extracting those features that are significant for predicting tool wear.

Figure 13 provides an overview of the feature extraction method. Initially, the database was segmented into nine patterns between the training and test data. Subsequently, tool life prediction using LightGBM was conducted for each dataset to calculate the importance of the features. The sum of the importance values calculated for each pattern was then computed, and the top 50 features with the highest sums were extracted. This selection of 50 items corresponds to the number of leaves in the LightGBM model used in this analysis, which limits the maximum number of features utilized in the prediction to 50. The right side of Fig. 13 illustrates the detailed process of calculating the sum of importance: the importance i of all features was calculated for each of the nine patterns, their sum i_{SUM} was computed, the features were then sorted in descending order based on the sum of importance, and the top 50 features were extracted.

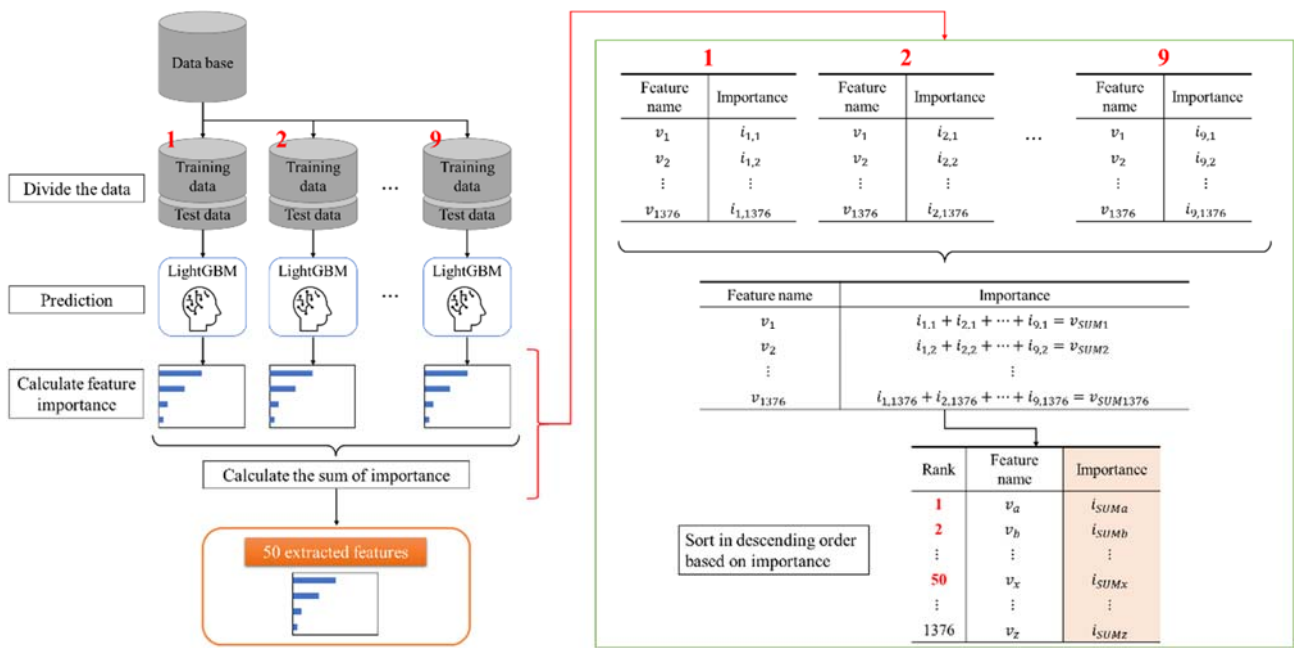


Fig. 13 Database segmented into two sets—training data and test data, each containing 9 patterns. Using LightGBM, tool life prediction is performed on both sets, and the significance of features is evaluated. Finally, the importance values of each feature for every pattern are summed up, and the top 50 features with the largest sum are extracted.

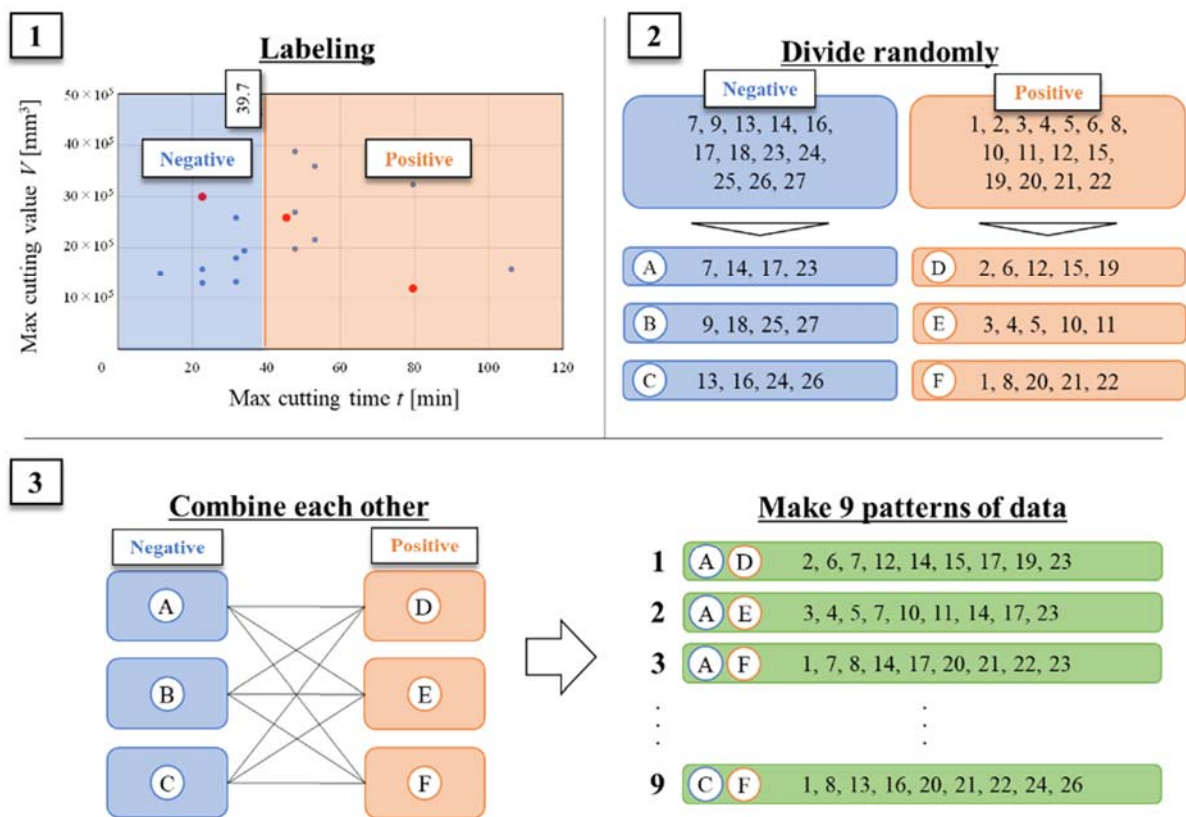


Fig. 14 This process is demonstrated in step 1 of the figure, using the tool life determination chart as an example. Specifically, the figure presents the results obtained when the threshold is set to $t = 39.7$.

Figure 14 details the procedure for creating the nine data division patterns. As depicted in step 1, a threshold of $t = 39.7$ min, for instance, is used in the tool life judgment diagram to divide the tool life point before and after the threshold (top left of the figure). In step 2, the cutting conditions (experiment numbers) are categorized into negative (NG) and positive (OK) based on the threshold. The experiment numbers refer to the current feature value obtained under each cutting condition. The current feature value of each category was randomly divided into three groups: NG (A, B, C) and OK (D, E, F). Thereafter, in step 3, the current value feature data from each category were combined to create a total of nine patterns of current feature value data, including each data point whose tool life point is near the threshold. These nine data patterns were further divided into training and test data for calculating feature importance in Fig. 14, with each pattern randomly assigned according to an 80% training data and 20% test data ratio.

4. Tool life prediction results and discussion using servo motor current value data under very early wear stage conditions

4.1 Prediction of tool wear from very early wear stage data in $\phi 12$ and $\phi 8$ square end-mill experiments

In this study, we initially predicted tool wear by analyzing the servo motor current data acquired during experiments with $\phi 12$ and $\phi 8$ square end-mills in the very early wear stage (cutting distance: 0–100 mm). As described in the experimental method Section 3.2, the work material for measurement was cut in a single pass (100 mm) while the tool was new at the beginning of each experiment. The prediction method assumes the use of servo motor current data from this stage, characterized by minimal tool wear. Therefore, the data from the first pass were utilized for analysis. The tool life judgment diagram for $\phi 12$ and $\phi 8$ square end-mills is illustrated in Fig. 15, where Fig. 11 distinguishes test data (red plots) and training data (blue plots). Figure 16 presents the data density in the horizontal and vertical axes of the tool life judgment diagram for the $\phi 12$ and $\phi 8$ square end-mill data, represented as histograms. A bubble chart in Fig. 16 indicates the number of data points per plot in the diagram, with plot size reflecting data quantity. The figure indicates that data density peaks at cutting times (t) and removal volumes (V) of 50–60 min and $19 \times 10^5 \text{ mm}^3$, respectively, where threshold values were also set.

The selection of test data followed two criteria:

- ① The data exhibit diverse cutting conditions, defined by the material removal rate (MRR [mm^3/min]), expressed as the product of table feed (F [mm/min]), radial depth of cut (ae [mm]), and axial depth of cut (ap [mm]). This diversity aimed to include test data under varied experimental conditions.
- ② The cutting conditions are those where the tool life is reached near the maximum cutting time 20–80 min and maximum removal volume 10×10^5 – $30 \times 10^5 \text{ mm}^3$, where the data density is concentrated in the data density histogram shown in Fig. 16.

These criteria were applied to select current value feature data from experiments 1, 8, and 27 of the $\phi 12$ square end-mill data for testing, as depicted in Fig. 15. Additionally, thresholds for maximum cutting time (t) and maximum removal volume (V) were set at 27, 40, 50, and 66 min for t , and 14×10^5 , 19×10^5 , 24×10^5 , and $29 \times 10^5 \text{ mm}^3$ for V . Thereafter, the system was validated in two patterns. In pattern (1), a database was created by extracting the top 50 feature items from the current value data during the very early wear stage for the $\phi 12$ and $\phi 8$ square end-mills, as described in Section 3.4. This database was used to test the data from experiments 1, 8, and 27 of the $\phi 12$ square end-mill. In pattern (2), validation involved using $\phi 10$ experimental data (extrapolated data) not included in the training data as test data.

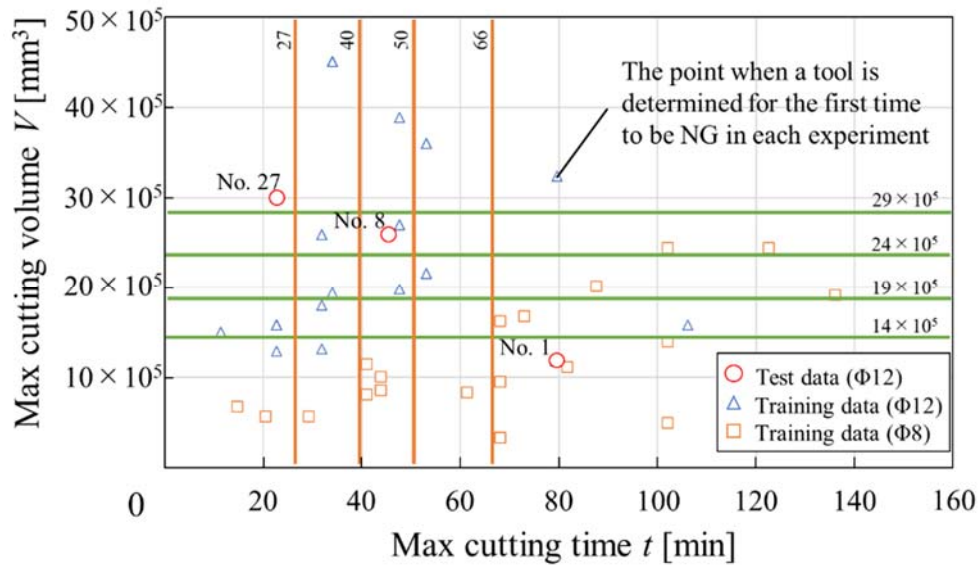


Fig. 15 Tool life evaluation for $\phi 12$ and $\phi 8$ square end-mills. Circle plots display the test data.

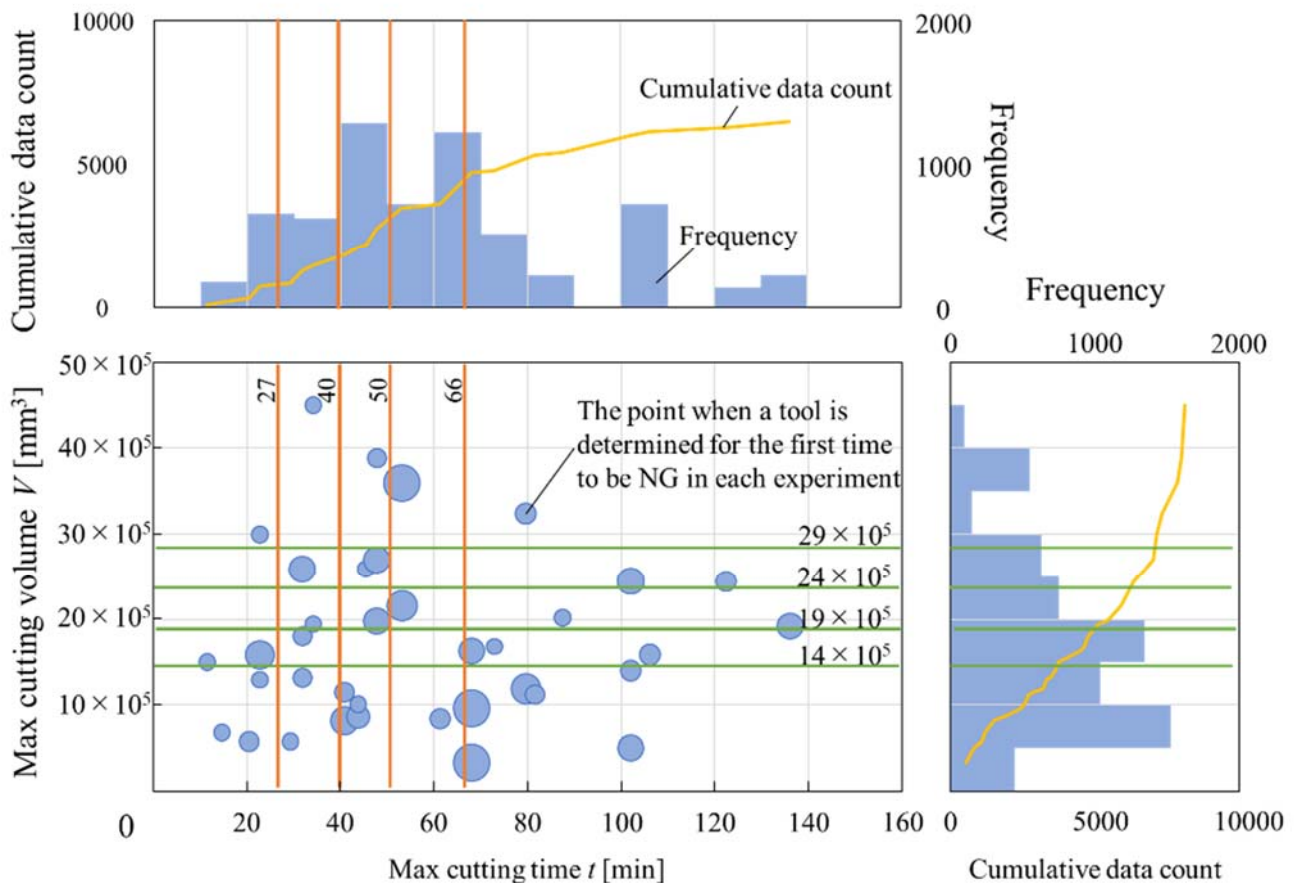


Fig. 16 Histograms display the data density on the horizontal and vertical axes for the tool life diagram utilized in the analysis of the $\phi 8$ and $\phi 12$ data extension.

The database information is detailed in Table 4 (a), and the total number of data existing in the range lower or higher than a threshold when the threshold is set as the boundary is presented in in (b). The table exhibits information regarding the database created from the $\phi 12$ and $\phi 8$ square end-mill experimental data, as well as the database when the $\phi 10$ experimental data are input as extrapolated data.

Table 5 presents the results of predicting tool wear state under two analysis patterns described previously. As explained in section 2.1, TPR was defined as the percentage of correctly predicted cases where tool wear life exceeded the threshold, whereas TNR denotes the percentage of correctly predicted cases where tool wear life did not exceed the threshold. For pattern (1), using maximum cutting time t as the threshold, the average ACR was 70.5%, TPR was 62.4%, and TNR was 64.6%. Specifically, for test data from cutting condition experiments 1 and 8 with a cutting time of 40 min or less (where tool life was not reached), the average TPR was 88.0%. For test data from experiments 8 and 27 with a cutting time of 50 minutes or longer (where tool life was reached), the average TNR was 90.95%. When the maximum removal volume V was the threshold, the average ACR was 67.0%, TPR was 84.0%, and TNR was 44.8%. With a removal volume threshold of $29 \times 10^5 \text{ mm}^3$ (as depicted in Fig. 15), only experiment 27 had not reached tool life, whereas experiments 1 and 8 had reached tool life, with TPR and TNR of 75.6% and 81.6% respectively. These results confirm that tool wear prediction is feasible with this system, regardless of the selected threshold. The above results confirmed that the tool wear prediction could be conducted using this system regardless of which threshold was selected.

Table 4 Database for tool life prediction

(a) Database information

		Pattern (1)	Pattern (2)
Data size		6483	6579
Feature size		50	50
Test data	Data size	318 (5%)	96 (1%)
	Note	$\phi 12$ condition No. 1,8,27	$\phi 10$ data No. 1-6
Training data	Data size	6165 (95%)	6483 (99%)
	Note	Others	

(b) Data Number (above threshold and subthreshold)

Threshold	Above threshold		Subthreshold	
	Pattern (1)	Pattern (2)	Pattern (1)	Pattern (2)
$t_{th} = 27[\text{min}]$	5,724	5,730	741	774
40[min]	5,034	5,022	1,449	1,482
50[min]	3,747	3,702	2,736	2,802
66[min]	2,895	2,754	3,588	3,750
$V_{th} = 14 \times 10^5 [\text{mm}^3]$	3,573	3,492	2,910	3,012
$19 \times 10^5 [\text{mm}^3]$	2,670	2,589	3,813	3,915
$24 \times 10^5 [\text{mm}^3]$	1,761	1,680	4,722	4,824
$29 \times 10^5 [\text{mm}^3]$	864	774	5,619	5,730

Figure 17 displays a graph of the most important features for predicting tool wear state across databases based on the results obtained from the $\phi 12$ end-mill experiment. The horizontal axis represents the importance value, and the vertical axis lists the feature names. The top features include wavelet coefficients (Cwt coefficients) and Fourier entropy. The graph also highlights a significant presence of Fourier coefficient features (FFT coefficients) among the top 10 features. Cwt coefficients are related to the wavelet transform used in frequency analysis. In this study, feature extraction with tsfresh involved extracting four types of features (real part, imaginary part, absolute value, angle) from a single frequency value, with the absolute value being utilized as the feature value.

The ratio value number to time series length, Lempel–Ziv complexity, and approximate entropy are quantitative measures that calculate the complexity of time series data. The Lempel–Ziv complexity utilizes the LZ700 data compression algorithm to express this complexity, while approximate entropy measures the reproducibility and

predictability of time series data.

For a spindle speed of $S = 5,322$ rpm, the top 10 FFT coefficient features included frequencies at 88, 89, and 161 Hz, which are approximately integer multiples of the base spindle speed of 88 Hz per second. During side cutting with an end-mill, the interaction between the tool cutting edge and the work material is intermittent. When the tool engages the work material, the machine tool increases power to the drive system to maintain the specified depth of cut. Thus, progressive tool wear alters the current value data when the dull tool cutting edge interacts with the work material at frequencies that are integer multiples of the spindle speed per second.

Consequently, as tool wear increases, so does the complexity of the time series data. This increase in complexity is reflected in the high values calculated for the Fourier coefficient features corresponding to these frequencies, which are significant for predicting tool life. Additionally, the complexity measures such as the ratio value number to time series length, Lempel–Ziv complexity, and approximate entropy also exhibit high values, indicating increased data complexity. This trend is consistent across other spindle speeds, including $\phi 8$.

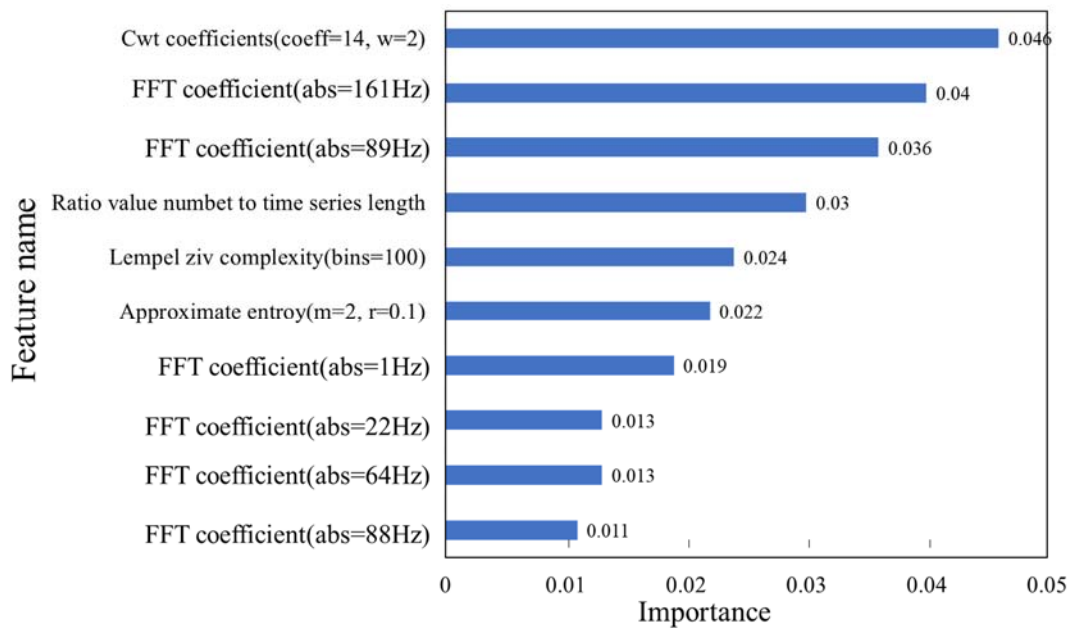


Fig. 17 Graph displays the top 10 most important features for tool life prediction for each database.

Table 5 Prediction results for tool life with threshold

(a) Prediction results when the threshold is time

Threshold	Result [%]	Pattern (1)	Pattern (2)	
$t_{th}[\text{min}]$	27	ACR	73.3	68.4
		TPR	89.0	100
		TNR	33.3	13.0
	40	ACR	75.2	67.6
		TPR	87.7	100
		TNR	43.3	10.6
	50	ACR	72.6	55.2
		TPR	58.9	47.9
		TNR	83.6	58.0
66	ACR	61.0	93.5	
	TPR	14.2	-	
	TNR	98.3	93.5	

(b) Prediction results when threshold is removal volume

Threshold	Result [%]	Pattern (1)	Pattern (2)	
$V_{th} \times 10^5$ [mm ³]	14	ACR	59.4	34.5
		TPR	100	81.3
		TNR	8.5	16.0
	19	ACR	55.7	71.7
		TPR	100	0
		TNR	0	100
	24	ACR	73.3	71.7
		TPR	60.5	0
		TNR	89.4	100
29	ACR	79.9	100	
	TPR	75.6	-	
	TNR	81.6	100	

4.2 Evaluation of prediction accuracy for extrapolated data

The tool wear prediction analysis previously described utilized current value data from the very early wear stage, employing experimental data that included the same tools in both the training and test datasets. In this section, we present the results of an analysis using experimental data obtained from tools that were not part of the training dataset, corresponding to pattern (2) as the test data. Specifically, the system was trained only on data from $\phi 8$ and $\phi 12$ square end-mills, while the $\phi 10$ square end-mill data, which were not included in the training, were used as extrapolated test data. As indicated in Table 4(a), the combined total of training and test data amounted to 6,579 entries.

Additionally, when the threshold values were set at $t = 66$ [min] for time and $V = 29 \times 10^5 \text{ mm}^3$ for volume, the TPR could not be defined because all tool life points in the test data dropped below these threshold values. From the results of Table 5, when the maximum cutting time t , was used as the threshold, the average ACR was 71.2%, the average TPR was 82.6%, and the average TNR was 43.8%. Conversely, when the maximum removal volume V , served as the threshold, the average ACR was 69.4%, average TPR was 27.1%, and average TNR was 79.0%.

Examining the results from the cutting experiments, the average TPR for the test data ($\phi 10$ end-mill cutting experiments numbers 1, 2, 4, and 5) was 100.0% at a cutting time of 40 [min] or less, where tool life was not reached. The average TNR for the test data ($\phi 10$ end-mill cutting experiments numbers 1 and 4) was 75.75% at a cutting time of 50 [min] or more, where tool life was reached. When the maximum removal volume threshold was set at $14 \times 10^5 \text{ mm}^3$, only cutting condition experiment number 6 in the test data had reached its tool life, resulting in a TPR of 81.3%. However, when the threshold was increased to $19 \times 10^5 \text{ mm}^3$ or $24 \times 10^5 \text{ mm}^3$, all test data except for cutting condition experiment number 4 had reached their tool life. At a threshold of $29 \times 10^5 \text{ mm}^3$, all test data reached their tool life, and from a threshold of $19 \times 10^5 \text{ mm}^3$ onwards, the TNR was 100.0%.

These results confirm that a system capable of predicting tool life at various thresholds can be effectively constructed, even with the inclusion of extrapolated data.

5. Conclusions

In this study, we transformed current value data collected from a servo motor, utilized as a machine tool during cutting processes, and employed the machine learning algorithm LightGBM to develop a predictive model for tool life based on early-stage wear data. The key findings of this research are summarized as follows:

- (1) The Fourier coefficient feature corresponding to the spindle speed per second was identified as a critical factor among the features derived from the current values of the servo motor in the initial stages of wear for predicting tool life.
- (2) The study demonstrated that by using the “very early wear stage” current feature values as test data, the cutting processing time and the material removal volume up to the future end of tool life can be predicted with an average accuracy of 70.5%.
- (3) The generalization performance of the proposed system was assessed by testing it with extrapolated data featuring a different tool diameter, which was not included in the training dataset. The results indicated that the average accuracy rates were 71.2% when using the maximum cutting time (t) and 69.4% when using the maximum removal volume (V) as thresholds.

Acknowledgments

This research was conducted with assistance from the METI Strategic Foundational Technology Improvement Support Operation (Support Improvement Program) “Development of a cutting tool management system (AI tool sommelier) that achieves smart factories using experiential knowledge of experts”. Mori Machinery Corp. also provided the cutting experiment environment for constructing the database. We express our gratitude for this support.

References

- Azeem, A., Determination of cutting parameters for peripheral end milling using discrete handbook data, *Journal of Mechanical Engineering*, Vol. 37, (2007), pp. 40-46.
- Dimla, D. E. and Lister PM, On-line metal cutting tool condition monitoring: I: force and vibration analyses, *International Journal of Machine Tools and Manufacture*, Vol. 40, No. 5, (2000), pp. 739-768.
- Ghosh, N., Ravi, Y. B., Patra, A., Mukhopadhyay, S., Paul, S., Mohanty, A. R. and Chattopadhyay, A. B., Estimation of tool wear during CNC milling using neural network-based sensor fusion, *Mechanical Systems and Signal Processing*, Vol. 21, No. 1, (2007), pp. 466-479.
- Jie, X., Yamada, K., Sekiya, K., Tanaka, R. and Yamane, Y., Comparison of applying static and dynamic features for drill wear prediction, *Journal of Advanced Mechanical Design, Systems, and Manufacturing*, Vol. 8, No. 4, (2014), pp. 1-8, DOI:10.1299/jamdsm.2014jamdsm0056.
- Kakino, Y., Ohtsuka, H., Nakagawa, H., Hirogaki, T. and Sasaki, M., A Study on Endmilling of Hardened Steel (1st Report) Simplified Prediction Model for Cutting Forces and Control for Constant Cutting Forces Using this Model, *Journal of Japan Society of Precision Engineering*, Vol. 66, No. 5, (2000), pp. 730-734 (in Japanese).
- Ke, G., Meng, Q., Finley, T., Wang, T., Chen, W., Ma, W., Ye, Q. and Liu, T. Y., LightGBM: A Highly Efficient Gradient Boosting Decision Tree, *Advances in Neural Information Processing Systems*, (2017), pp. 3146-3154.
- Krishnakumar, P., Rameshkumar, K. and Ramachandran, K. I., Acoustic emission-based tool condition classification in a precision high-speed machining of titanium alloy: a machine learning approach, *International Journal of Computational Intelligence and Applications*, Vol. 17, No. 3, (2018), DOI:10.1142/S1469026818500177.
- Li, X., Djordjević, A. and Venucinod, P. K., Current-Sensor-Based Feed Cutting Force Intelligent Estimation and Tool Wear Condition Monitoring, *IEEE Transactions on Industrial Electronics*, Vol. 47, No. 3, (2000), pp. 697-702.
- Li, X., Du, R., Denkena, B. and Imiela, J., Tool Breakage Monitoring Using Motor Current Signals for Machine Tools with Linear Motors, *IEEE Transactions on Industrial Electronics*, Vol. 52, No. 5, (2005), pp. 1403-1408.
- Li, Y., Meng, X., Zhang, Z. and Song, G., A Machining State-Based Approach to Tool Remaining Useful Life Adaptive Prediction, *Sensors*, Vol. 20, No. 23, (2020), DOI:10.3390/s20236975.
- Liu, C., Zhang, L., Niu, J., Yao, R. and Wu, C., Intelligent prognostics of machining tools based on adaptive variational mode decomposition and deep learning method with attention mechanism, *Neurocomputing*, Vol. 417, No. 5, (2020), pp. 239-254.
- Mahmood, J., Mustafa, G. and Ali, M., Accurate estimation of tool wear levels during milling, drilling, and turning operations by designing novel hyperparameter tuned models based on LightGBM and stacking, *Journal of the International Measurement Confederation*, Vol. 190, No. 28, (2022), DOI:10.1016/j.measurement.2022.110722.
- Nie, L., Zhang, L., Xu, S., Cai, W. and Yang, H., Remaining Useful Life Prediction of Milling Cutters Based on CNN-BiLSTM and Attention Mechanism, *Symmetry*, Vol. 14, (2022), DOI:10.3390/sym14112243.
- Nouri, M., Fussell, B. K. and Ziniti, B. L., Real-time tool wear monitoring in milling using a cutting condition independent method, *International Journal of Machine Tools and Manufacture*, Vol. 89, (2015), pp. 1-13.
- Rizal, M., Ghani, J. and Nuawi, M. A., A review of sensor system and application in milling process for tool condition monitoring, *Res. J. Appl. Sci. Eng. Technol.*, Vol. 7, (2014), pp. 2083-2097.
- Salimi, A., Zadeshakoyan, M., Ozdemir, A. and Seidi, E., Drill Wear Prediction System Using of Motor Current and Fuzzy Logic Method, *Iranian Journal of Materials Science and Engineering*, Vol. 9, No. 2, (2012), pp. 15-29.
- Wang, Q., Wang, H., Hou, L. and Yi, S., Overview of Tool Wear Monitoring Methods Based on Convolutional Neural Network, *Applied Science*, Vol. 11, No. 24, (2021), pp. 1-24.